Interface Wave Contribution to Acoustic Particle Motion During Offshore Wind Farm Construction

16

Gopu R. Potty, James H. Miller, Ying-Tsong Lin, and Kathleen J. Vigness-Raposa

Contents

Abstract

Construction of offshore wind turbines, via impact pile driving, generates and radiates intense acoustic and sediment borne energy through the water column and ocean bottom. The acoustic waves generated by impact pile driving include interface (Scholte) and shear waves in the ocean bottom in addition to compressional waves in the water column and sediments. The particle motion component of acoustic energy is particularly important to fishes and invertebrates. Scholte waves contribute significantly to the particle motion generated in the seabed and have maximum amplitude at the seafloor. Scholte wave contribution to the measured data is identified using Random Decrement technique in this study. Data measured during the construction of the Coastal Virginia Offshore Wind (CVOW) project are analyzed. The CVOW project involved the construction of two 6- megawatt wind turbines located 43 km east of Virginia Beach, Virginia. The turbines were pinned to the seabed using mono piles of diameter 7.8 m. A suite of particle motion sensors, including Ocean Bottom Recorders (OBX),

G. R. Potty (✉) · J. H. Miller
Department of Ocean Engineering, University of Rhode Island, Narragansett, RI, USA
e-mail: gpotty@uri.edu; miller@uri.edu

Y.-T. Lin
Woods Hole Oceanographic Institution, Woods Hole, MA, USA
e-mail: ytlin@whoi.edu

K. J. Vigness-Raposa
INSPIRE Environmental, Newport, RI, USA
e-mail: kathy@inspireenvironmental.com

A. N. Popper et al. (eds.), *The Effects of Noise on Aquatic Life*,
https://doi.org/10.1007/978-3-031-50256-9_126

was deployed to monitor the acoustic pressure and particle velocity on the seabed during December 2021 to January 2022. To examine the potential effects of sound on fishes and invertebrates, the behavioral thresholds and behavioral audiograms of some of these animals to the particle motion component of sound were compared to the measured data. These measurements were part of the Bureau of Ocean Energy Management (BOEM) sponsored Real-time Opportunity for Development Environmental Observations (RODEO) Program [Work supported by Bureau of Ocean Energy Management (BOEM)].

Keywords

Offshore wind farm · Scholte wave · Particle motion · RODEO · Coastal Virginia Offshore Wind

Introduction

The quest for renewable sources of energy has led to the increase in the development of offshore wind farms over the last decade. Most of the current offshore wind farm developments are in shallow waters (less than approximately 30–50 m) and the preferred method of construction in shallow waters is either using a single cylindrical tower (monopile) or jacket type of structure. Installation of either of these wind turbine substructures requires driving piles into the seabed. Pile driving generates acoustic and seismic waves in the air, water column, and the seabed. Generation of Mach waves during impact hammer pile driving and its propagation characteristics has been well studied and described in Reinhall and Dahl (2011), Potty et al. (2011), Kim et al. (2022), Miller et al. (2016), Wilkes and Gavrilov (2017), and Amaral et al. (2020a). The acoustic energy radiated from the pile directly and reflected from the boundaries of the waveguide contributes significantly to the sound received at any distance from the pile in the water column. The contribution of sound produced during any construction of offshore wind farms can change the underwater soundscape and alter the habitats of marine mammals, fishes, and invertebrates by potentially masking communications or causing mortality, permanent threshold shift (PTS), temporary threshold shift (TTS), or behavioral disturbances for species that rely on sound for mating, navigating, and foraging (Amaral et al. 2020b).

In addition to the sound pressure generated in the water, compressional, shear, and interface waves are generated in the seabed that propagate outward from the pile in all directions (Amaral et al. 2020b). Compressional waves (P-waves) are the fastest traveling waves in the seafloor and are characterized by particle motion that is parallel to the direction of wave propagation, whereas shear waves (S-waves), which are slower than P-waves, have particle motion that is perpendicular to the direction of the propagating wave (Amaral et al. 2020b). Interface waves travel along the water-sediment interface at a speed about 90% of the shear waves with maximum particle motion amplitude at the interface (Kolsky 1963). Interface waves along the water-sea bottom boundary are called Scholte waves. The particle motion amplitude

of Scholte waves will have maximum amplitude at the interface and will decay exponentially away from the interface both in the water column and seafloor. Hence the effect of these types of waves will be felt only within one or two wavelengths from the seafloor. The low-frequency and slow-moving Scholte waves propagate over long distances and can generate large-amplitude oscillations along the water-sediment boundary. These Scholte waves have the potential to affect marine life that are sensitive to this type of disturbance living close to or within the seafloor sediment (Popper and Hawkins 2018).

Research interest in understanding the role of sound in the functioning of aquatic ecosystems, and the ways in which sound affects animal behavior and physiology, has gained increased attention in the recent past. While aquatic mammals use acoustic pressure, many fishes and invertebrates detect and use the acoustic particle motion (Nedelec et al. 2016). Since many aquatic animals sense particle motion, this component of the sound field should be taken into account while assessing the impact of the acoustic field on the environment. Measurements and model predictions of particle motion are few compared to acoustic pressure data, and experimental data on the response of fishes and invertebrates to particle motion are also scarce.

Many invertebrates appear to respond to vibrations (Roberts and Elliot 2017); for example, the bivalve *Scrobicularia plana* (peppery furrow shell) is sensitive to vibration and may therefore react to the foot-fall of its predator *Haematopus ostralegus* (oystercatcher). The anemone *Anthopleura elegantissima* (aggregating anemone) and the sea urchin *Strongylocentrotus purpuratus* (purple sea urchin) can detect vibrations within the frequency range of waves on the shore. Within the seabed, there is evidence to suggest that *Rimicaris exoculate* (deep sea shrimp) detect falling prey using vibration, and flatfish such as *Pleuronectes platessa* (European plaice) and *Solea* spp. may use vibrations to sense predators (Roberts and Elliot 2017). Roberts et al. (2016) conducted a study aimed to determine to what extent the common marine intertidal hermit crab, *Pagurus bernhardus* L. (Family Paguridae) is sensitive to substrate-borne vibration, and to fully define the sensitivity range and behavioral responses in relation to levels produced by anthropogenic activities. They presented results of this study along with published values of behavioral thresholds to vibration (both in water and substrate-borne) for crustaceans for comparison (Roberts et al. 2016).

Acoustic pressure and particle motion measurements were made during the construction phase of the Coastal Virginia Offshore Wind (CVOW) project. The CVOW project, which consists of two 6- megawatt wind turbines, is located 43 km east of Virginia Beach, Virginia. These measurements were made using Ocean Bottom Recorders (OBX) along with many other sensor systems. Four OBXs were deployed as a linear array, and data from one of the OBX are analyzed in the present study. Panel c in Fig. 1 shows the picture of an OBX and the axes definitions. The particle velocities are measured along these axes (x, y, and z directions), and acoustic pressure is measured on a hydrophone co-located with the directional sensors. The OBX sampled the data at 2 kHz during the CVOW deployment. In addition to the acoustic/seismic measurements, the OBX package also has a heading sensor which

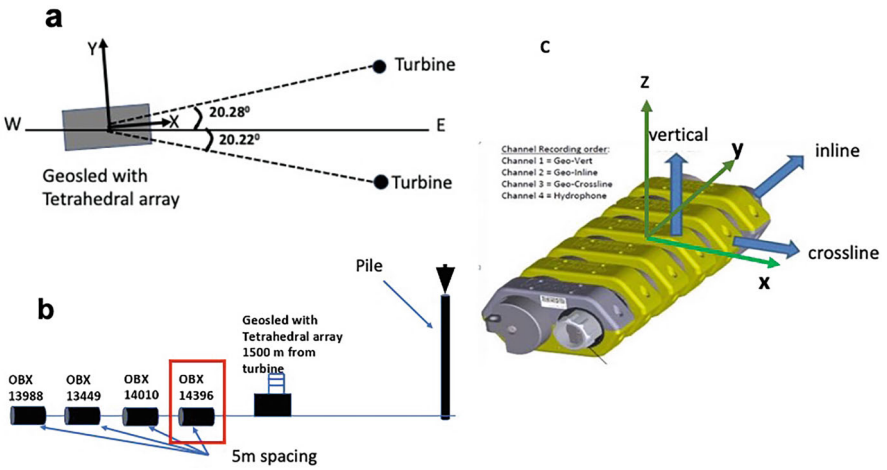

Fig. 1 (**a**) Position of the OBXs in relation to the two CVOW turbines. The dashed line indicates the propagation path from the turbine to the OBX. (**b**) Geometry of the four OBXs which were attached to a sled. The sled was located at 1500 m from the pile driving locations. The spacing of the OBXs was 5 m. (**c**) Picture of an Ocean Bottom Recorder (OBX) with the axis definitions. Particle velocities are measured along the x, y, and z directions

measures the heading information that is used to properly orient the OBX, in the horizontal plane, in order to calculate the direction of arrival of acoustic signals. The CVOW turbines were installed on monopile type substructure (7.8 m diameter) with piles driven by impact hammer strikes. Locations of the OBX sensor packages in relation to the two turbines are shown in Fig. 1 (panels a and b). No bubble curtains were used during the construction of the north turbine whereas noise mitigation measures (bubble curtain) were used during construction of the south turbine. Based on the triangulated positions of the OBXs, the propagation of acoustic energy from the piles should arrive at 20° angle to the East (as shown in Fig. 1; panel a). The range from the pile to the OBX considered in this study is approximately 1500 m. This range was the closest distance from the turbine where deployments were permitted based on safety considerations.

Figure 2 (left panel) shows particle velocity measured on the first OBX sensor in the array (OBX 14396, highlighted by the red box in Fig. 1; panel b) during pile installation. Data shown in Fig. 2 correspond to the north turbine in which no sound reduction methods (i.e., no bubble curtain) were used during pile driving operations. Figure 2 shows approximately 1 minute of data during which approximately 50 hammer strikes were recorded. Each impulse in the figure correspond to one hammer strike. Upper panel on the left in Fig. 2 shows the vertical component of the particle velocity (in mm/s) whereas the lower panel shows the radial component (along the propagation path in the horizontal plane).

The radial component of velocity is obtained by projecting the X and Y components of the particle velocity components along the propagation path from the turbine to the OBX (shown in Fig. 1; panel a). The radial velocity is approximately

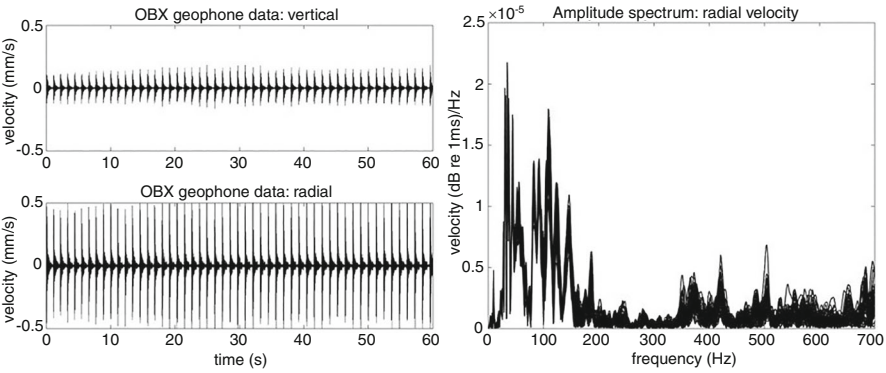

Fig. 2 Particle velocity measured on the OBX sensor (left panel). Upper panel on the left shows the vertical component of the particle velocity (in mm/s) whereas the lower panel shows the radial component (along the propagation path in the horizontal plane). Right panel shows the amplitude spectrum of the radial velocity component

five times larger than the vertical velocity. Since the OBX is deployed on the seabed, it will measure shear and interface waves in addition to the compressional waves. This makes the OBX data complicated and identification of the contribution of the different wave types will be helpful in interpreting the data. The interface waves will have the maximum amplitude at the seabed; its amplitude decays exponentially away from the interface and cylindrically in range. The right panel in Fig. 2 shows the amplitude spectrum of the radial component of velocity from all 50 events shown on the left, showing the energy distribution as a function of frequency. The frequency content in the different events appears to be very similar showing very little spread in the spectral amplitudes especially at low frequencies. These low frequencies (below 200 Hz) seem to dominate the spectrum.

A technique known as Random Decrement (RayDec) approach is used to identify the Scholte wave arrivals in the data (radial and vertical components shown in Fig. 2). The RayDec approach provides the frequency band in which the Scholte wave arrivals dominate and the direction of arrival (DOA) of these arrivals. The RayDec algorithm calculates the frequencies and DOA of Scholte wave arrivals by searching the data (the vertical and horizontal components of velocity) at various times and frequencies and identifying the 90° phase shift between them (vertical and horizontal components) which is a characteristic feature of the Scholte wave particle motion (Hobiger et al. 2009; Potty et al. 2022).

Figure 3 shows the time-frequency distribution of acoustic energy (top left panel) calculated using wavelet-based analysis and the direction of arrival of Scholte waves (top right panel) calculated using the RayDec algorithm. The portion of the time series (six seconds long with five hammer strikes) which was used to create the time-frequency representations of acoustic energy and azimuth is also shown in bottom right. The time series analyzed corresponds to data from the north turbine (without bubble curtain). Azimuth estimates with a confidence level of 60% and above are only shown in the top right panel. Scholte wave arrivals can be seen in the frequency

band from 30 Hz to 90 Hz. Most of the arrivals, in the band 30 Hz to 70 Hz (indicated by blue color), appear to come at an angle of 20° north of the east-west direction. Arrivals can also be seen at 20 Hz and above 70 Hz which appears to come from different angles. This could indicate a different source (low-frequency micro-seismic energy) or coming through different interfaces/paths. There is also a 10 Hz and 60 Hz spectral component (left panel) which is present throughout and possibly not related to the hammer impact events.

The particle velocity and acceleration amplitudes at the measurement location, 1500 m from the turbines, are significant and have the potential to impact the behavior of fishes and invertebrates. The particle acceleration levels can be compared to the behavioral thresholds to assess the potential for impacts as shown in Table 1. The values shown are acceleration levels in dB re 1 μm/s^2 at four different

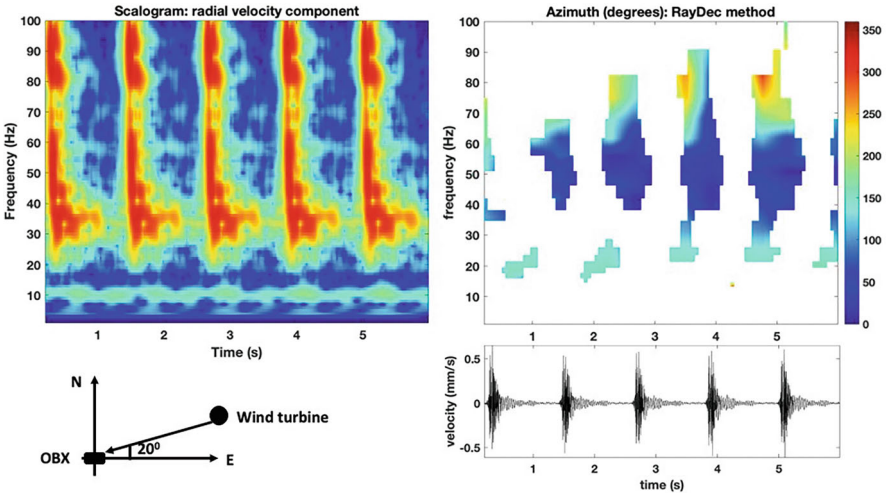

Fig. 3 Time-frequency distribution of acoustic energy (top left panel) and direction of arrival of Scholte waves (top right) of the section of data (bottom right) analyzed. The propagation path from the north turbine to the OBX is indicated in the bottom left panel

Table 1 Behavioral audiogram thresholds for fishes and behavioral response thresholds for a crustacean to vibration. Values taken from the literature and compared to CVOW data (Popper et al. 2014; Roberts et al. 2016). Bold numbers indicate threshold values lower than the CVOW levels. The values shown are acceleration levels in dB re 1 μm/s^2 at four different frequencies

	30 Hz	35 Hz	45 Hz	83 Hz
Atlantic salmon	**41.33**	**41.1**	**40.7**	**38.5**
Dab	**33.33**	**33.33**	**35.58**	**28.8**
Atlantic cod	**31.33**	**28**	–	–
Plaice	**28.87**	**27.44**	**25.42**	**22.97**
Atlantic sand fiddler	**70.1**	**72.04**	75.56	81.93
CVOW data	*71.5*	*73.7*	*73.7*	*76.8*

frequencies in the band where the acoustic energy is maximum (as shown in Fig. 3). The behavioral audiograms of four fishes (Atlantic salmon, dab, Atlantic dod and plaice) are taken from Popper et al. (2014), whereas the behavioral response threshold values for *Uca pugilator* (Atlantic sand fiddler) is calculated based on values from Roberts et al. (2016). Last row in Table 1 shows the acceleration level measured from the CVOW data as shown in Fig. 2. The threshold values are highlighted in bold numbers if they are lower than the measurement at different frequencies. The measured data are higher than the audiogram threshold values for all of the fishes considered. It indicates they can hear the sound, but whether that will lead to any behavioral changes in fishes is impossible to conclude without behavioral threshold values. The measured levels are slightly higher at two frequencies in the case of *Uca pugilator* (Atlantic sand fiddler) behavioral response threshold.

It should be noted that the results shown in Figs. 2 and 3 and Table 1 correspond to data from the north turbine which did not have a bubble curtain. The bubble curtain did reduce the acoustic energy produced by hammer impacts at the south turbine (with bubble curtain) measured on the OBXs. Figure 4 shows the comparison of the spectra of the data measured on OBX (indicated on Fig. 1 with a red box). As can be seen from Fig. 4, the received particle velocity (both vertical and radial components) levels drops by approximately 10 dB, for frequencies higher than 300 Hz, when bubble curtains were employed. At low frequencies (frequencies less than 300 Hz) the bubble curtain performs not as effectively as at higher frequencies. This frequency dependent performance of the bubble curtain is being investigated in detail currently by analyzing data from other receivers and through modelling.

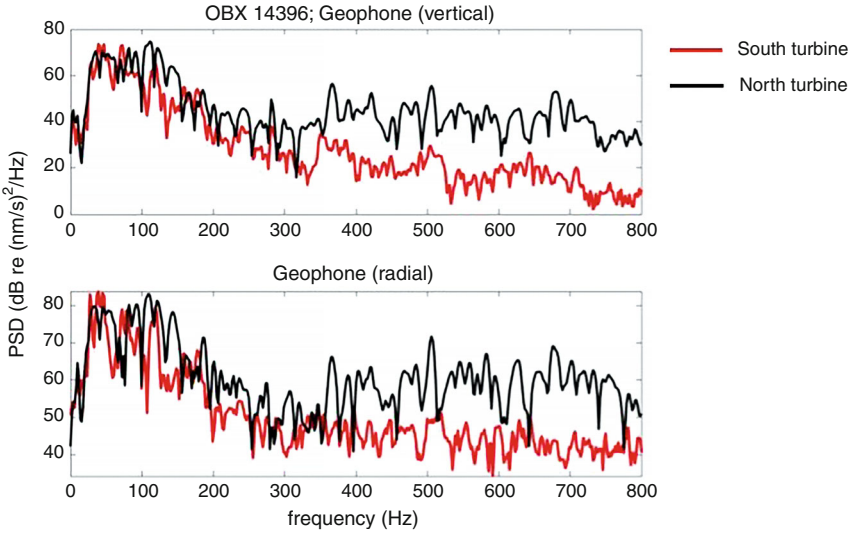

Fig. 4 Power spectrum of OBX geophone data from the north turbine (black) and south turbine (red). The pile driving for the north turbine was done without bubble curtains whereas the south turbine employed bubble curtain

Conclusions

The contribution of Scholte waves to the particle motion measured on the seabed at a range of 1500 m from impact pile driving operations was assessed in this study. The frequencies and direction of arrival of Scholte waves were identified using RayDec technique. The acceleration levels measured were also compared to behavioral audiograms and thresholds of some fishes and a crustacean. Preliminary comparisons indicate that the fishes and crustaceans considered in this study could hear or be behaviorally impacted by the pile driving operations at 1500 m.

Acknowledgments Study concept, oversight, and funding for the experiment were provided by the U.S. Department of the Interior, Bureau of Ocean Energy Management (BOEM), Environmental Studies Program, Washington, DC under Contract Number M15PC00002, Task Order M16PD00025. The OBX system was acquired under a DURIP grant. Collaborators in this project include Anwar Khan and Kristen Ampela (HDR, Inc.), Arthur Newhall (WHOI), and Tim Mason (Subacoustech., UK).

References

Amaral JL, Miller JH, Potty GR, Vigness-Raposa KJ, Frankel AS, Lin Y-T, Newhall AE, Wilkes DR, Gavrilov AN (2020a) Characterization of impact pile driving signals during installation of offshore wind turbine foundations. J Acoust Soc Am 147(4):2323–2333. https://doi.org/10.1121/10.0001035

Amaral J, Vigness-Raposa KJ, Miller JH, Potty GR, Newhall A, Lin Y-T (2020b) The underwater sound from offshore wind farms. Acoust Today 16(2):13–21. https://doi.org/10.1121/AT.2020.16.2.13

Hobiger M, Bard P-Y, Cornou C, Le Bihan N (2009) Single station determination of Rayleigh wave ellipticity by using the random decrement technique (RayDec). Geophys Res Lett 36:L14303

Kim H, Miller JH, Potty GR, Amaral J (2022) Long-range propagation modelling of offshore pile driving noise based on the configuration of the support structure. In: Proceedings of the 24th International Congress on Acoustics (ICA2022), Gyeongju, Korea

Kolsky H (1963) Stress waves in solids. Dover Publications, New York

Miller JH, Potty GR, Kim H-K (2016) Pile-driving pressure and particle velocity at the seabed: quantifying effects on crustaceans and groundfish. In: Popper AN, Hawkins AD (eds) The effects of noise on aquatic life II. Springer, New York, pp 719–728

Nedelec SL, Campbell J, Radford AN, Simpson SD, Merchant ND (2016) Particle motion: the missing link in underwater acoustic ecology. Methods Ecol Evol 7:836–842

Popper AN, Hawkins AD (2018) The importance of particle motion to fishes and invertebrates. J Acoust Soc Am 143:470–488. https://doi.org/10.1121/1.5021594

Popper AN, Hawkins AD, Fay RR, Mann DA, Bartol S, Carlson TJ, Coombs S, Ellison WT, Gentry RL, Halvorsen MB, Lokkeborg S, Rogers PH, Southall BL, Zeddies DG, Tavolga WN (2014) ASA S3/SC1.4 TR-2014 Sound exposure guidelines for fishes and sea turtles, Springer briefs in oceanography. Springer, Cham. https://doi.org/10.1007/978-3-319-06659-2_3

Potty GR, Kim H, Miller JH (2011) Acoustic radiation from offshore wind farms. In: 2011 international symposium on ocean electronics, Kochi, India, pp 178–184. https://doi.org/10.1109/SYMPOL.2011.6170519

Potty GR, Miller JH, Bonnel J, Lin Y-T, Knobles DP, Wilson PS (2022) Preliminary inversions using compressional, shear and interface waves in the New England Mudpatch. In: Proceedings of the International Congress on Acoustics (ICA2020), Gyeongju, Korea

Reinhall PG, Dahl PH (2011) Underwater Mach wave radiation from impact pile driving: theory and observation. J Acoust Soc Am 130(3):1209–1216. https://doi.org/10.1121/1.3614540

Roberts L, Elliot M (2017) Good or bad vibrations? Impacts of anthropogenic vibration on the marine epibenthos. Sci Total Environ 595:255–268

Roberts L, Cheesman S, Elliot M, Breithaupt T (2016) Sensitivity of *Pagurus bernhardus* (L.) to substrate-borne vibration and anthropogenic noise. J Exp Mar Biol Ecol 474:185–194

Wilkes DR, Gavrilov AN (2017) Sound radiation from impact-driven raked piles. J Acoust Soc Am 142:1–11. https://doi.org/10.1121/1.4990021